JBC RESEARCH ARTICLE

# Molecular counting of myosin force generators in growing filopodia

Received for publication, May 25, 2024, and in revised form, October 7, 2024 Published, Papers in Press, October 28, 2024,
https://doi.org/10.1016/j.jbc.2024.107934

**Gillian N. Fitz and Matthew J. Tyska***

*From the Department of Cell and Developmental Biology, Vanderbilt University School of Medicine, Nashville, Tennessee, USA*

Reviewed by members of the JBC Editorial Board. Edited by Enrique De La Cruz

**Animal cells build actin-based surface protrusions to enable diverse biological activities, ranging from cell motility to mechanosensation to solute uptake. Long-standing models of protrusion growth suggest that actin filament polymerization provides the primary mechanical force for "pushing" the plasma membrane outward at the distal tip. Expanding on these actin-centric models, our recent studies used a chemically inducible system to establish that plasma membrane–bound myosin motors, which are abundant in protrusions and accumulate at the distal tips, can also power robust filopodial growth. How protrusion resident myosins coordinate with actin polymerization to drive elongation remains unclear, in part because the number of force generators and thus, the scale of their mechanical contributions remain undefined. To address this gap, we leveraged the SunTag system to count membrane-bound myosin motors in actively growing filopodia. Using this approach, we found that the number of myosins is log-normally distributed with a mean of 12.0 ± 2.5 motors [GeoMean ± GeoSD] per filopodium. Together with unitary force values and duty ratio estimates derived from biophysical studies for the motor used in these experiments, we calculate that a distal tip population of myosins could generate a time averaged force of ∼tens of pN to elongate filopodia. This range is comparable to the expected force production of actin polymerization in this system, a point that necessitates revision of popular physical models for protrusion growth.**

Filopodia are fingerlike, micron-scale, membrane protrusions that extend from the surface of diverse eukaryotic cell types (1). Structural support for these features is provided by a cytoskeletal core containing 10 to 30 actin filaments, cross-linked by the actin bundling protein fascin (2) and uniformly oriented with their fast growing barbed-ends against the plasma membrane at the filopodial tip. Filopodia are found in a range of physiological scenarios, where they enable cells to physically and biochemically interact with neighboring cells and the external environment. In tissues as diverse as mesenchymal cells and neurons, filopodia are critical for cell migration, cell-cell contact formation, and wound healing (3–5). Despite their widespread appearance, important questions surrounding the physical basis of filopodial formation remain open.

Cell biological studies and mathematical models dating back several decades suggest that mechanical force generated by the elongation of actin filaments drives the outward deformation of membrane required for filopodial formation (6–8). Here, a balance between the force generated by the fast-growing, barbed ends of actin filaments ($F_{BE}$) and the mechanical barrier provided by tension in the overlying plasma membrane ($F_{MEM}$) dictates whether a distal tip elongates ($F_{BE} > F_{MEM}$), stalls ($F_{BE} = F_{MEM}$), or retracts ($F_{BE} < F_{MEM}$). However, given the actin-rich nature of filopodia and related structures such microvilli and stereocilia, members of the myosin superfamily of actin-based force generators are abundant protrusion residents that could shift the mechanical balance between polymerization and membrane tension (9–11). In vertebrates, myosins that contain MyTH4-FERM cargo-binding domains offer specific examples, including Myo10 in filopodia (12), Myo7B in microvilli (13), and Myo15A and Myo7A in stereocilia (14, 15). The functions of these motors are ancient and likely conserved given that myosins with similar structural motifs also contribute to filopodial formation in lower eukaryotes (16). Previous studies established that MyTH4-FERM myosins use the core actin bundle as a track to drive tipward transport of cargoes that are needed for protrusion growth and long-term stability (1). Myo10 is a highly studied case; as a processive motor that accumulates at filopodial tips, this motor delivers protein and lipid cargoes that promote filopodia formation, stability, and anchoring (12, 17–22). Indeed, a recent screen using the C-terminal FERM domain of Myo10 as bait identified numerous proteins with wide ranging functions in signaling and regulating cytoskeletal dynamics (17).

In addition to carrying cargo *via* their C-terminal tails, protrusion resident myosins also interact with the plasma membrane, either directly or indirectly (1), suggesting that these motors could impact the force balance that controls protrusion elongation. Our group recently tested this concept using a genetically encoded, chemically inducible system, which enabled precise temporal control of myosin motor domain recruitment to the plasma membrane. Activation of this system led to rapid and robust elongation of numerous filopodia (23). This effect was supported by motor domains from structurally distinct MyTH4-FERM domain containing myosins, different membrane-binding motifs, and was

* For correspondence: Matthew J. Tyska, matthew.tyska@vanderbilt.edu.

operational in distinct cell types. These experiments revealed that, beyond powering the tipward transport of cargoes, myosin motors can also contribute to protrusion growth by applying barbed-end-directed force to the overlying plasma membrane and potentially shifting the balance of force to favor filopodial growth ($F_{BE} > F_{MEM}$). We now refer to this myosin-powered, filopodial induction system as 'filoForm', a name inspired by the plant species *filiformis*, which generates large numbers of long, thin protrusive structures on its leaves; this nomenclature also links to previous filopodia-themed resources adopted by the cytoskeleton field (24–26).

The question of how myosin-generated force promotes protrusion growth remains open. One possibility is that applying tipward force to the plasma membrane increases actin polymerization efficiency by making the fast-growing barbed ends of filaments more accessible for monomer incorporation. Such an effect could be mediated by driving the tipward flow of lipids, which might decrease local membrane tension within the filopodial tip compartment. Alternatively, myosin-generated force might accelerate retrograde flow of the core actin bundle, which could, similarly, make the barbed ends of core bundle actin filaments more accessible, allowing for more efficient polymerization. Although these ideas are intuitive, the mechanistic details of how membrane-bound myosins promote protrusion growth remain unclear due to the lack of quantitative information on the number of force generators (actin *versus* myosin) that are active in individual protrusions during growth.

To address this gap, we leveraged our ability to initiate the formation of filopodia with filoForm in combination with a single molecule imaging strategy to directly count the number of myosin motors in individual, newly formed filopodia. Using this approach, we found that the number of motors that accumulate in the distal tip compartment during filopodial elongation was highly variable, even across the surface of an individual cell, with a mean of 12 motors per filopodium. Using this value to estimate time-averaged force production, a myosin population of this scale could generate ∼ tens of pN, comparable to the expected force production by elongating barbed ends of core bundle actin filaments. The results reported here will be critical for constraining physical models of protrusion growth that consider mechanical contributions from both force generating systems: actin filaments and protrusion resident myosins.

## Results

### Combining SunTag18x and filoForm to enable counting of myosin molecules in filopodia

To count myosin force generators in elongating filopodia, we first sought an approach that would enable visualization and tracking of single myosin molecules. To this end, we took advantage of the SUperNova (SunTag) system, a tandem GCN4 repeat scaffold that recruits mulitple copies of GFP (single-chain variable fragment scFV fused with superfolder GFP) through antibody–peptide interactions (27). The SunTag greatly enhances the fluorescence signal emitted from single-tagged molecules, such that conventional imaging methods, including spinning disk confocal microscopy (SDCM), can be used for visualization. Since its creation, the SunTag system has been used to visualize a range of dynamic cellular processes in live cells, including the motion of single kinesin motors along microtubules in U2OS cells, synaptic vesicle transport in cultured neurons, and gene translation in living *Drosophila* embryos (28–30). Our intent in the current study was to combine the high signal/noise ratio offered by the SunTag with the inducible myosin-driven system of filopodial growth, filoForm, described in our previous work (Fig. 1*A*) (23). FiloForm is a genetically encoded system that takes advantage of the rapalog-inducible heterodimerization of FRB and FKBP to dock force-generating myosin motors to the plasma membrane *via* a membrane-binding motif, CDHR2TM (Fig. 1*B*). In the minutes that follow activation with rapalog, cells undergo robust filopodial elongation. In combining SunTag and filoForm (SunTag-filoForm), our goal was to activate filopodial growth and simultaneously monitor the number of myosin motors that accumulate in growing protrusions (Fig. 1*C*).

Our previous experiments with filoForm established that myosin-driven filopodial growth is supported by motors with diverse biochemical properties, from classes 3, 10, and 15 (23). For the current studies, we focused specifically on myosin-10 motor domain (Myo10MD) as a model myosin force generator. Because the larger variants of the SunTag with many tandem GCN4 repeats are predicted to be bulky and hold some risk of impairing function, we first set out to determine the shortest GCN4 linker that would still enable single molecule visualization using SDCM, while also supporting filopodial elongation. Testing a range of constructs composed of increasing numbers of tandem GCN4 repeats (4x, 8x, 12x, 14x, 16x, 18x, 20x, and 24x) revealed that 18xGCN4 tag (SunTag$_{18x}$) offered the best compromise between high brightness and robust induction of filopodial growth following rapalog addition (Fig. 1, *D* and *E*; Video S1).

### Defining the fluorescence intensity of a single Myo10MD molecule

HeLa cells transfected with SunTag$_{18x}$-Myo10MD-FRB (referred to herein as Myo10MD) were subject to volume imaging with SDCM, which enabled us to capture filopodia in their entirety. We first sought to measure the intensity of individual Myo10MD puncta in the cytoplasm prior to inducing filopodia elongation with rapalog addition. To measure single Myo10MD punctum intensities unaffected by diffusive motion, we acutely depleted cells of ATP to lock myosin motors in a long-lived (*i.e.,* rigor-like) actin-bound state (Fig. 2*A*). To gradually deplete cytoplasmic ATP, we treated HeLa cells with 0.05% sodium azide and 10 mM 2-deoxy-D-glucose (31) and then imaged the ventral cell surface using SDCM. Within 15 min of ATP depletion, new Myo10MD puncta landed and dwelled for many frames in the imaging plane, presumably reflecting strong binding to basal actin fibers (Fig. 2, *B* and *C*; Video S2). Using TrackMate (32), we quantified the sum pixel intensities of single Myo10MD puncta that entered and

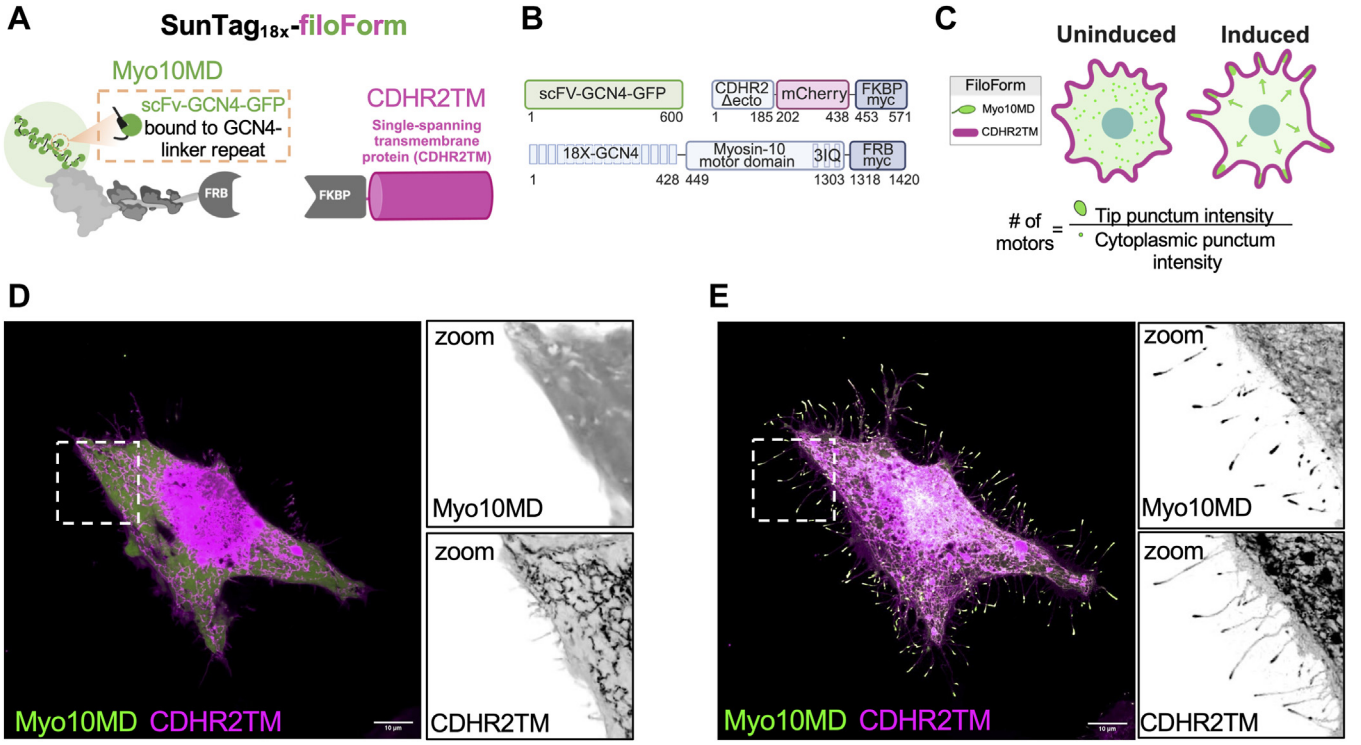


**Figure 1. Single molecule confocal imaging using SunTag$_{18x}$-filoForm.** *A*, schematic of the antibody-peptide labeling strategy (SunTag$_{18x}$) to amplify the signal of single Myo10MD molecules combined with the inducible filoForm system, where FRB–FKBP interactions dock the motor to the membrane anchor (CDHR2TM) upon the addition of rapalog. *B*, cartoons depicting the three constructs that comprise SunTag$_{18x}$-filoForm that were transfected into cells to induce filopodia elongation; numbers represent amino acids. *C*, graphic of the functional output of these experiments; Myo10MD signal intensity at induced filopodia tips was calibrated by the intensity of cytoplasmic single molecule Myo10MD puncta to calculate the number of motors in each induced filopodium. *D*, confocal maximum intensity projection image of a HeLa cell expressing the SunTag$_{18x}$-filoForm system before rapalog addition. *E*, confocal maximum intensity projection image of a HeLa cell expressing SunTag$_{18x}$-filoForm 30 min after rapalog induction. Scale bar = 10 μm. Myo10MD, myosin-10 motor domain.

remained in focus for at least 15 frames (discarding transient events). Any nonspecific clustering of tagged Myo10MD molecules within observed the diffraction-limited puncta would lead us to overestimate the fluorescence signal per molecule. However, previous optimization of SunTag motifs minimized aggregation (27), and the distribution of single punctum intensities that we observed here was well fit to a single Gaussian (Fig. 2*D*), suggesting a monodispersed population of fluorescent molecules. Thus, the puncta observed in our images most likely represent single tagged Myo10MD molecules. Next, we averaged the sum intensities from many Myo10MD puncta per cell (28, 32); subtracting background from these values yielded a mean Myo10MD punctum intensity of 320 12 bit gray values (Fig. 2*E*), which we subsequently used as a calibration factor for counting Myo10MD motors in growing filopodia as described below.

### *Newly elongated filopodia contain tens of Myo10MD molecules*

To quantify the number of Myo10MD motors that accumulate in newly formed filopodia, we induced filopodia elongation using SunTag$_{18x}$-filoForm, performed volume imaging with SDCM, and used 3D thresholding to quantify the sum intensity of motor signal at the distal tips, 30 min after rapalog activation. Using the single molecule calibration value determined above, we found that filopodia contained 12 myosin motors per protrusion (12.0 ± 2.5 motors, GeoMean ± GeoSD), although induced protrusions demonstrated significant variability, containing as few as two and as many as 349 motors (Fig. 3*A*). We were curious to determine how these values compared to protrusions generated by the overexpression of wildtype Myo10, which is known to drive robust filopodial initiation and elongation (12). To test this, we created a full-length Myo10 (Myo10FL) construct tagged with SunTag$_{18x}$ (Fig. 1). We transfected HeLa cells with SunTag$_{18x}$-Myo10FL and again used SDCM to examine motor accumulation at filopodial tips. Given the nature of conventional transient transfection experiments, the population of protrusions that we analyzed in this case contained both nascent and mature filopodia. 3D thresholding and intensity analysis revealed that filopodia tips in Myo10FL expressing cells contained ∼9 myosin motors per protrusion (Fig. 3*B*), comparable to what we observed using the filoForm described above. Thus, independent of the mode of myosin-dependent filopodia assembly (induced *versus* stochastic), filopodia contain ∼ tens of motors (Fig. 3*B*).

### *Filopodia dynamics are impacted by the number of tip localized Myo10MD molecules*

Next, we wondered if the dynamic properties of growing filopodia are impacted by the number of myosin motors that accumulate at the distal tips. To investigate this possibility, we

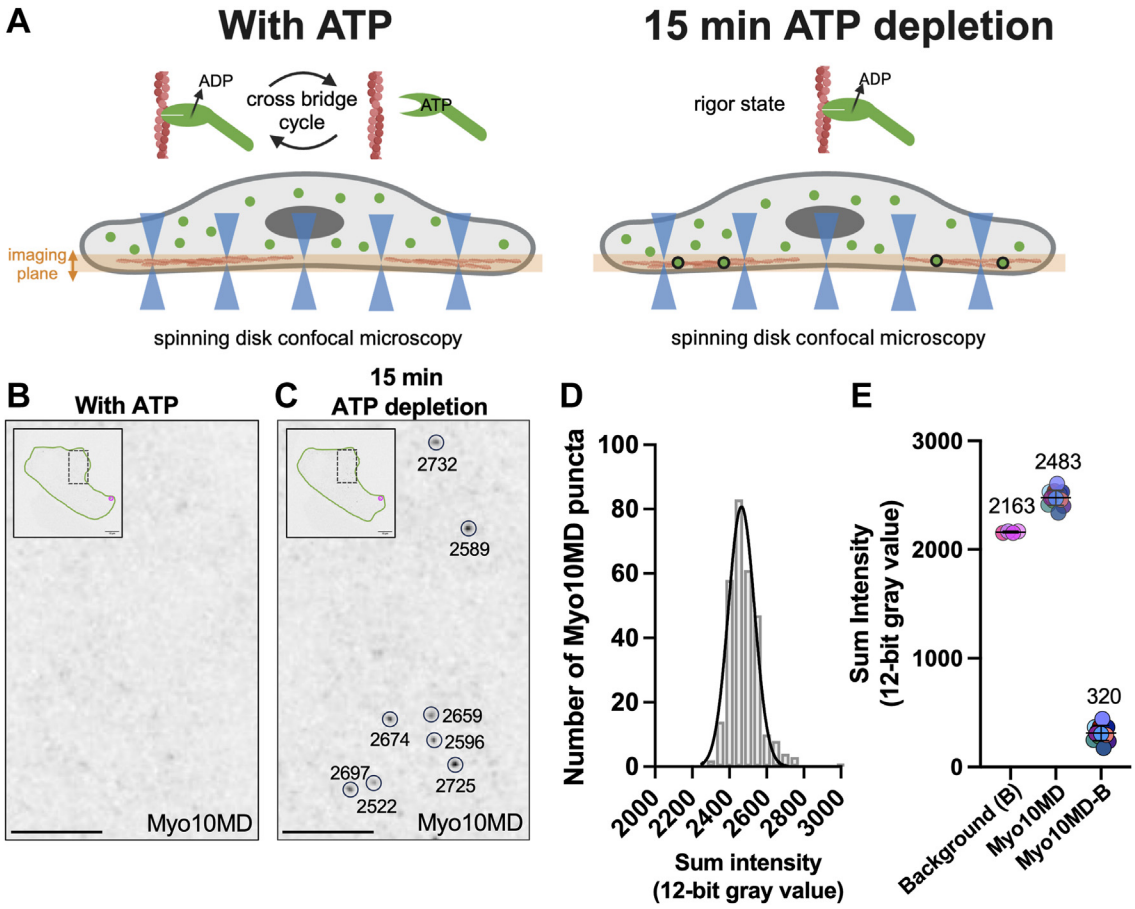


**Figure 2. Calibrating the fluorescence intensity of single Myo10MD molecules.** *A*, schematic of ATP depletion experiments used to immobilize Myo10MD molecules. Upon ATP depletion, myosin motors become strongly bound to actin in a rigor state, which increases the number of motors in a single z-plane (*A* and *B*, *orange band*). *B*, zoomed image of the ventral surface of a HeLa cell expressing Myo10MD (inverted; *black*) before ATP depletion; inset shows the cell body outlined in *green*. *C*, zoomed image of the ventral surface of a HeLa cell expressing Myo10MD (inverted; *black*) 15 min after ATP depletion. Cell body is outlined in *green*; eight puncta are *circled* and shown with the measured sum intensities. Scale bars in B and C = 5 μm. *D*, histogram of the sum intensities of 292 individual Myo10MD puncta from 13 cells; curve fit is a single Gaussian with mean = 2465, S.D. = 70.4, and amplitude = 80.7; $R^2$ = 0.97. *E*, sum intensities of Myo10MD puncta from ATP depleted cells; each dot represents the average sum intensity of all puncta measured per cell. For background, n = 100 puncta; for Myo10MD, n = 292 puncta from 13 cells. Plotted values represent the intensity of background (*B*), Myo10MD puncta, and Myo10MD puncta with background subtracted (-B); bars show mean ± S.D. Myo10MD, myosin-10 motor domain.

imaged the elongation of nascent filopodia at low z-resolution for 30 min and then acquired high-resolution volumes to enable the counting of myosin motors as described above (Fig. 4*A*). We then generated trajectories from distal tip motion during elongation to calculate the elongation rate, persistence of elongation, and maximum final length for each filopodium. Using the GeoMean of 12 as a threshold, we binned trajectories into low and high motor groups, which had population means of 6.0 ± 0.3 and 45.0 ± 5.4 motors, respectively (mean ± sem). Filopodia in the high motor group elongated faster (low, 0.6 ± 0.3 μm/min *versus* high, 0.7 ± 0.2 μm/min) (Fig. 4*B*) were more persistent (low, 0.5 ± 0.2 *versus* high, 0.6 ± 0.2) (Fig. 4*C*) and reached longer final lengths (low, 4.0 ± 2.0 μm *versus* high, 5.3 ± 2.9 μm) (Fig. 4, *D* and *E*). While the increases in tip velocity and persistence were subtle, the most significant increase was observed in the final length of filopodia. These results suggest that force generated by membrane-bound myosins probably delays the stalling of growth that ultimately limits filopodia length.

## Discussion

Our recent work established that membrane-bound myosins can tilt the force balance at filopodial tips to promote elongation, presumably by potentiating the force generated by core bundle actin filaments (23). To define the scale of myosin motor force production, we combined the SunTag with the filoForm system, which allows for both single molecule visualization and inducible control of filopodia formation *via* the docking of myosin motors to the plasma membrane. The primary advance offered by our approach is that measurements are time-resolved, allowing us to focus our analysis on actively growing filopodia immediately after induction of the filoForm system.

Monitoring myosin accumulation in newly grown filopodia revealed that only ∼12 myosin motors are needed to induce the rapid elongation of protrusions. When we overexpressed a SunTagged variant of Myo10FL and examined intensities at filopodia tips in live cells ∼24 h post transfection, we obtained a similar result with a mean of ∼9 motors per filopodium.

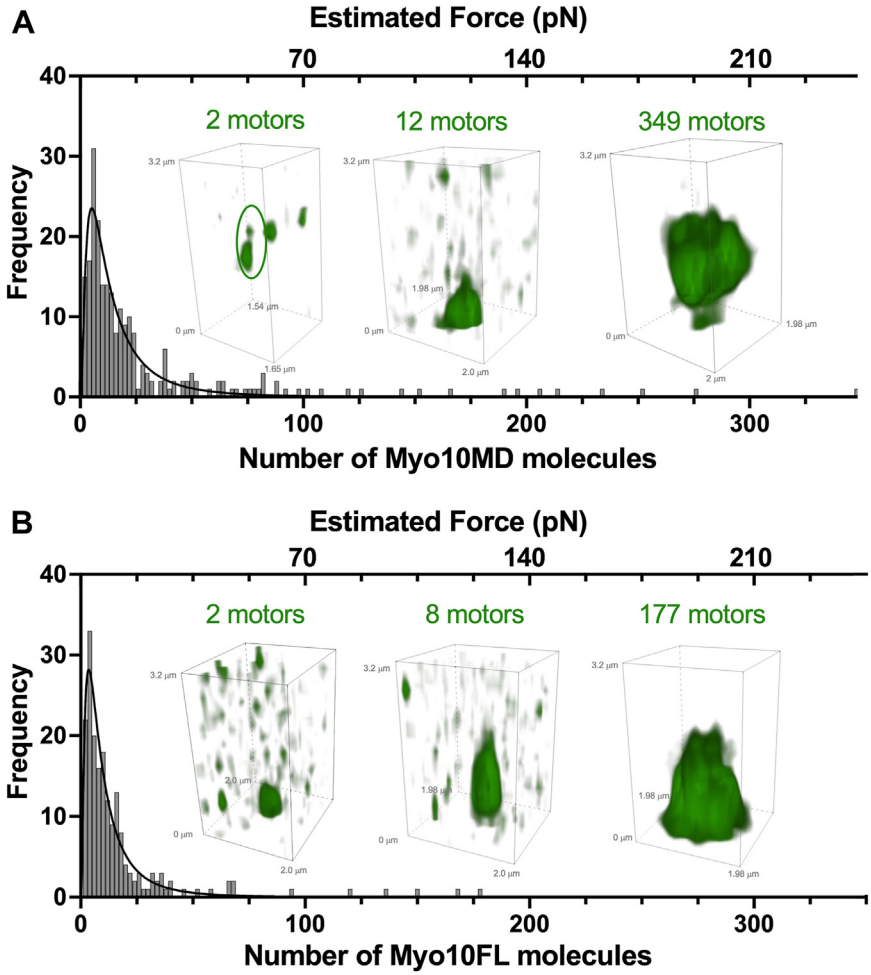


**Figure 3. Newly formed filopodia contain tens of Myo10MD molecules.** *A*, distribution of the number of Myo10MD molecules counted at the tips of newly formed filopodia using $SunTag_{18x}$-filoForm; curve fit represents a log-normal distribution with 12.0 ± 2.5 motors (GeoMean ± GeoSD). *Green* inset images depict deconvolved volume projections of filopodial tips showing a range of motor numbers; n = 14 cells, 237 individual filopodial tips. *B*, distribution of the number of Myo10FL molecules at filopodial tips 24 h post transfection; curve fit represents a log-normal distribution with 8.6 ± 2.6 motors (GeoMean ± GeoSD). *Green* inset images depict deconvolved volume projections of filopodial tips showing a range of motor numbers; n = 18 cells, 189 individual filopodia. For both *A* and *B*, top x-axis represents the correlating level of estimated force calculated using a duty ratio of 0.7 and unitary force of 1 pN. Myo10FL, full-length Myo10; Myo10MD, myosin-10 motor domain.

Although we know with certainty the age of nascent protrusions that grow after activating the filoForm system, we are unable to know the age of filopodia formed by full-length Myo10 given the stochastic nature of protrusion growth in those experiments. Nevertheless, filopodia in the latter case are expected to be older on average relative to induced protrusions. Thus, filopodial aging (or maturation) does not appear to significantly change the number of myosin motors in the distal tip compartment. This point further implies that the number of myosins promoting elongation may be set at the initiation of filopodial growth. In contrast to our findings, a recent study in U2OS cells demonstrated that overexpression of Myo10FL leads to filopodial tips that contain hundreds of motors (median of ∼360 molecules), with a large range around this value (2–65,000 molecules) (33). Although we employed a direct single molecule visualization strategy, that study used a population level biochemical approach combined with epifluorescence microscopy to approximate the number of motors in individual cells, and in turn, single filopodia. Interestingly, the authors did describe a population of filopodia characterized by dim tip puncta, representing only tens of Myo10 motors, which would be generally consistent with the results we present here.

How much mechanical force could ∼ tens of myosin motors generate at the tip of a filopodium? The time-averaged force ($F_{avg}$) produced by a population of motors is related to the number of force generators in the population (in this case ∼12), the unitary force produced by individual motors ($F_{uni}$ ∼1 pN), and the duty ratio, *i.e.,* the fraction of the total ATPase cycle spent in a force-generating state ($F_{AVG}$ = $F_{UNI}$ × # of motors × duty ratio) (34). Duty ratio estimates for the Myo10 motor used in our studies are wide ranging (0.16–0.7) (35, 36), but the higher value of 0.7 yields $F_{AVG}$ of ∼8.4 pN (35). Notably, this calculation does not consider the lifetime of the membrane-bound state for force generating myosins, although this is expected to be long for motors activated in the filoForm system, given the strong binding interactions between the rapalog and FKBP/FRB modules (37). Because native

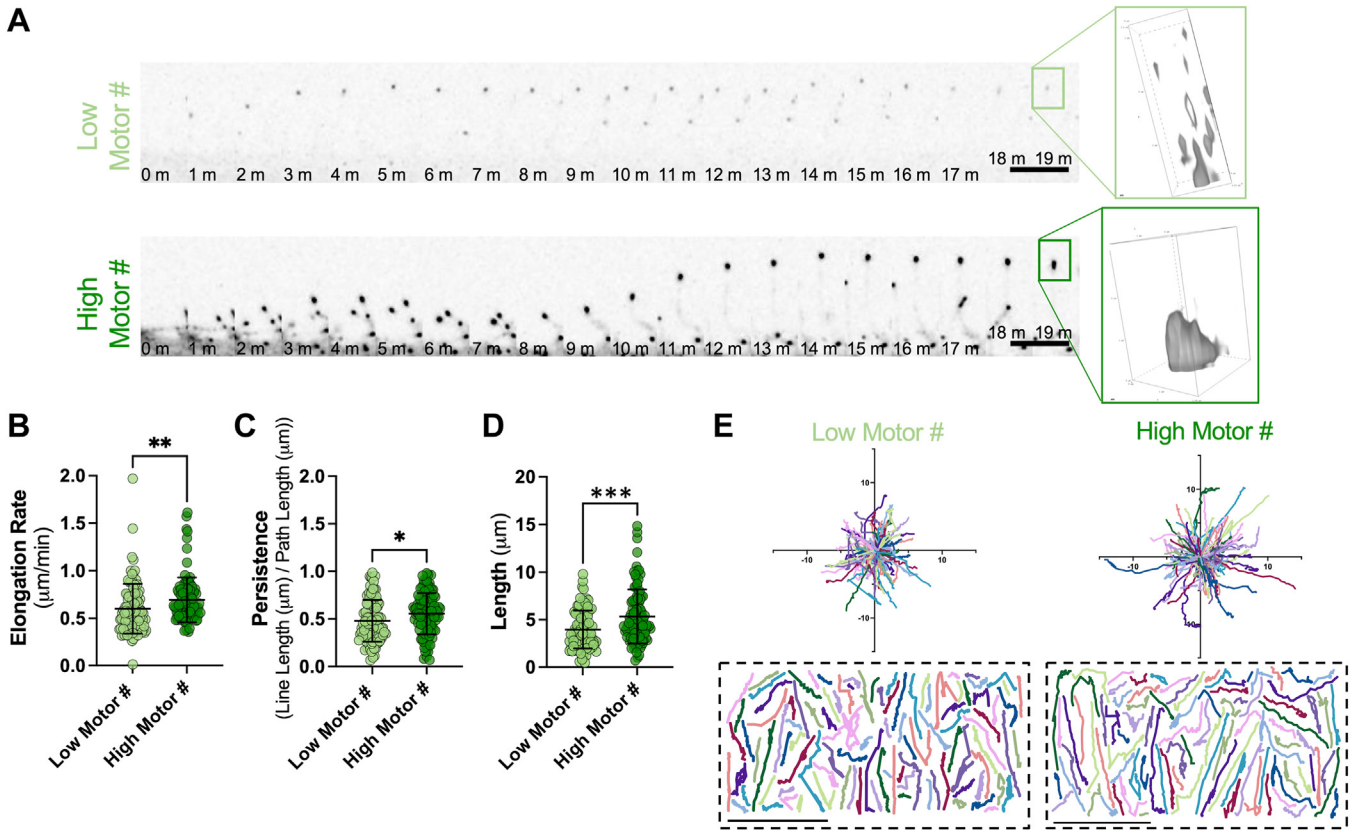


**Figure 4. Filopodial growth dynamics depend on the number of tip targeted myosin motors.** *A*, timelapse montage of individual filopodia induced by SunTag$_{18x}$-filoForm containing a low (2; *top*) or high (47; *bottom*) numbers of myosin motors. *Right*, deconvolved volume projections of the filopodial tips at the final time point. Scale bar = 5 μm; LUTs matched to high motor montage. *B–D*, quantification of (*B*) elongation rate, (*C*) persistence of elongation, and (*D*) final length for filopodia containing low (<12, *light green*) or high (>12, *dark green*) numbers of motors (6.0 ± 0.3 and 45.0 ± 5.4 motors, respectively). Error bars represent the mean ± SD; *$p \leq 0.05$, **$p \leq 0.05$, ***$p \leq 0.001$, n = 100 (*low*) and 102 (*high*). *E*, *rose plots* of individual trajectories of filopodial tips containing *low* (<12; *light green*) or high (>12; *dark green*) numbers of motors. *Dashed boxes* below depict the individual filopodial tracks. Scale axis = 10 μm.

protrusion myosins probably bind/unbind the membrane at a higher frequency, the value of $F_{AVG}$ derived above may represent an overestimate.

How does $F_{AVG}$ generated by tip targeted myosins compare to the force generated by elongating actin filaments in the filopodium ($F_{BE}$)? Previous biophysical studies established that polymerizing actin filaments exert up to ∼1 pN on an opposing surface (6, 38). Filopodia core bundles assembled in neurons contain up to ∼20 filaments (39), putting an average maximum force generated by that mechanism at ∼20 pN. However, growing barbed-ends of a parallel bundle are unlikely to exhibit synchronous and continuous insertion of new actin monomers (40), and therefore the number of filaments exerting force on the plasma membrane at any point in time will likely be a fraction of the total number. With this in mind, the level of force generated by actin and membrane-bound myosins during filopodial elongation may be within the same order of magnitude.

Analysis of filopodia containing high *versus* low numbers of myosin motors revealed that more motors increased filopodial elongation rate, persistence, and length, although the changes in these parameters were subtle. Given that filoForm system constructs are overexpressed, it is possible that limiting levels of endogenous components (*e.g.*, actin filaments, ATP, and plasma membrane lipids) restricted the impact of larger Myo10MD motor populations on filopodial dynamics. To begin to examine this possibility, we used phalloidin staining to probe the amount of actin polymer in individual protrusions and then attempted to correlate that value to the number of motors measured in each structure. However, this analysis failed to reveal a clear correlation (data not shown), suggesting that the number of actin filaments and myosin motors may be uncoupled in actively growing filopodia. If this is true, then in certain protrusions, the number of Myo10MD motors might exceed the number of binding sites offered by the core actin bundle, and in those cases, higher motor numbers would have less of an impact on filopodial dynamics.

The number of myosin motors that accumulated at the tips of newly grown filopodia was highly variable, even across the surface of a single cell (Fig. S1, *A* and *B*). What does this observation suggest about factors that control protrusion growth? One possible explanation is linked to local variability in membrane tension. Based on popular models of filopodia formation, in-plane tension in the plasma membrane is viewed as the primary physical barrier that growing actin filaments must contend with to elongate these structures (7, 41). In the

context of our assays, membrane tension could vary from cell to cell (*e.g.,* based on overall morphology or surface attached area) or across the surface of an individual cell. Consistent with this latter possibility, previous biophysical studies established that membrane tension does vary locally, with single cells yielding a wide range of tether forces (∼5–30 pN) depending on where the tether is pulled (41–43). From this perspective, the large variability in distal tip myosin accumulation within individual cells might reflect variability in local membrane mechanics, with regions of high and low tension across the surface requiring higher or lower levels of myosin force production, respectively, for filopodial elongation. Another possibility relates to inherent variation in the local accumulation of other factors that promote filopodia growth. This idea is supported by a recent study from Gallop *et al*., which revealed striking variability in the composition of filopodial tip complexes and further highlighted that stochastic accumulation of different combinations of factors are able to support filopodial growth (44).

While generating and optimizing SunTagged myosin motor constructs, we noted that the 24xGCN4 tag (SunTag$_{24x}$) was unable to elongate filopodia. One explanation is that this longer variant was unable to acquire a stable fold and therefore remained nonfunctional in the cytoplasm. However, a more intriguing possibility is that the longer variant was too bulky to enter the tight confines of the space between the actin core and the encapsulating plasma membrane, at the filopodial base. Although a size-exclusion limit has not yet been reported for filopodia, we examined solved structures and AlphaFold predictions to estimate the volumes occupied by the tagged myosin constructs used in our studies (Fig. S2) (45, 46). The volumes of a single Myo10MD tagged with FRB, a single EGFP, and a single scFV bound to a GCN4 motif are ∼130 nm$^3$, ∼29 nm$^3$, and ∼72 nm$^3$, respectively. Extrapolating these values leads to approximate volumes for EGFP-Myo10MD-FRB, 20xGCN4-Myo10MD-FRB, and 24xGCN4-Myo10MD-FRB of ∼159 nm$^3$, ∼1568 nm$^3$, and ∼1855 nm$^3$, respectively. Are these molecular volumes too large to enter the space between the actin core bundle and overlying plasma membrane at the base of a newly forming filopodia? Cryo-TEM images of *Dictyostelium* filopodia offer an estimate of the distance between the core actin bundle and encapsulating membrane of ∼15 nm (47), and a sphere with this diameter would occupy ∼1767 nm$^3$. Using this value as a molecular volume threshold, one would predict that 24XGCN4-Myo10MD-FRB (∼1855 nm$^3$) would be unable to gain access to filopodia and this matches our observations. Although these results are consistent with the idea that access to a filopodium may be restricted based on molecular volume, future studies working with native filopodial resident proteins will need to explore this possibility further.

In conclusion, our investigations revealed that newly forming filopodia only require tens of myosin motors to elongate. A population of this scale could generate force ($F_{AVG}$) at a level comparable to that produced by polymerizing filament barbed ends ($F_{BE}$) and therefore make a significant contribution toward overcoming the physical barrier that impedes filopodial growth ($F_{MEM}$). The large variability in motor numbers between protrusions further reinforces the previously described mosaicism of mechanisms that drive protrusion growth (44). Importantly, these findings necessitate updates to popular physical models of filopodial growth, which generally consider polymerizing actin filaments as the sole force generators in these structures.

## Experimental procedures

### Lead contact

Further information and requests for resources and reagents should be directed to and will be fulfilled by the lead contact, Matthew J. Tyska (matthew.tyska@vanderbilt.edu).

### Materials availability

Plasmids generated in this study will be made available from the lead contact on request.

### Experimental model and subject details

#### Cell culture

HeLa cells were cultured at 37 °C and 5% $CO_2$ in Dulbecco's modified Eagle's medium (DMEM) (Corning #10–013-CV) with high glucose and 2 mM L-glutamine supplemented with 10% fetal bovine serum (FBS). Transfections were performed using Lipofectamine 2000 (Thermo Fischer #11668019) according to the manufacturer's protocol. For live imaging, cells were plated in 35mm glass-bottom dishes (Cellvis #D35–20–1.5-N).

#### Cloning and constructs

All PCR reactions and site-directed mutagenesis were performed with Q5 High-Fidelity DNA Polymerase (NEB #M0491S). EGFP-Myo10MD-FRB and the single-spanning transmembrane domain membrane docking construct (CDHRTM-mCherry-FKBP) were used as previously described (23). To fuse GCN4 linkers of different lengths (4x, 8x, 12x, 16x, 18x, 20x, and 24x) to Myo10MD-FRB, we replaced the EGFP from EGFP-Myo10MD-FRB with GCN4 repeats from pHRdSV40-K560-24xGCN4_v4 (Addgene #72229) *via* Gibson assembly (NEB #E2621S) using the primer sets listed below. Finally, we generated a variant of scFV-GFP by removing the nuclear localization sequence *via* an early stop codon from pHR-scFv-GCN4-sfGFP-GB1-NLS-dWPRE (Addgene #60906) with the following primers: 5′- tggtagctgaggtggtactagtcccaagaagaagc-3′ and 5′-ccacctcagctaccaccaccttcggttacc-3'. The reaction was then digested with DpnI (NEB #R0176S) to remove template plasmid, retaining only the mutagenized plasmid that contained the early stop codon.

(24x) 5′- acccaagctgggccaccatggaagaacttttgagcaagaattatcatct tgagaacgaagtg-3′

5′- attcgagatctgagtccggacttttttaagtcgggctacttcattctcgaga-3′

(20x) 5′-acccaagctgggccaccatggaagaacttttg-3′

5′- attcgagatctgagtccggacttctttagtcgagccacctcgttctcg -3′

(18x) 5′- acccaagctgggccaccatggaagaactttgagcaagaattatcatcttgagaacgaagtg-3′
5′- attcgagatctgagtccggatttcttcaagcgggcgact -3′
(16x) 5′- acccaagctgggccaccatggaagaactttgagcaagaattatcatctgagaacgaagtg -3′
5′- attcgagatctgagtccggatttttgagcctggcgacttca -3′
(14x) 5′- acccaagctgggccaccatggaagaactttgagcaagaattatcatcttgagaacgaagtg -3′
5′- attcgagatctgagtccggatttcttcaatctcgcgacctcattc -3′
(12x) 5′- acccaagctgggccaccatggaagaactttgagcaagaattatcatcttgagaacgaagtg -3′
5′- attcgagatctgagtccggatttctttaagcgcgcgacttcgttctctaaatgatag -3′
(8x) 5′- acccaagctgggccaccatggaagaactttgagcaagaattatcatcttgagaacgaagtg-3′
5′- attcgagatctgagtccggatttctttaatcgagctacttcgttttcgagg -3′
(4x) 5′- acccaagctgggccaccatggaagaactttgagcaagaattatcatcttgagaacgaagtg -3′
5′- attcgagatctgagtccggacttttttagccgagccacttcgttt -3′

### *Drug treatments*

To induce heterodimerization of FRB and FKBP constructs, transfected cells were treated with 500 nM of A/C Heterodimerizer (Takara #635057) at the onset of live imaging. For ATP depletion experiments, transfected HeLa cells were switched to glucose-free DMEM (Fischer #11–966–025) supplemented with 2 mM L-glutamine and 10% FBS. Before the onset of live cell imaging, 0.05% sodium azide (Fischer #11–966–025) and 10 mM 2-deoxy-d-glucose (Sigma #D3179) were added. To minimize lateral waving of filopodia, 0.5% methylcellulose diluted in DMEM with high glucose and 2 mM L-glutamine supplemented with 10% FBS were added prior to imaging.

### *Light microscopy and image processing*

Live imaging was performed on a Nikon Ti2 inverted light microscope equipped with a Yokogawa CSU-W1 spinning disk head, 405 nm, 488 nm, 561 nm, and 647 nm excitation LASERs, a 100X Apo TIRF 100x/1.45 NA objective, and a Photometrics Prime 95B sCMOS camera. Cells were maintained in a stage top incubator at 37 °C with 5% CO2 (Tokai Hit). For measurements of puncta intensity, a single z-stack was acquired with exposures of 50 ms per frame prior to depleting ATP. ATP depletion media were then added, and 15 min later, the same cells were imaged for 5 s. For imaging the tips of induced filopodia, a 0.5 μm z-stack was acquired, and rapalog was added to induce filopodia elongation, and after 30 min, a two-color volume of the same cell was acquired using a 3 μm z-stack (15 × 0.2 μm z steps with 60 ms exposures). For imaging to quantify the dynamic properties of filopodial elongation, transfected cells were imaged every 15 s for 30 min using a 0.5 μm z-stack. At the end of 30 min, another 3.0 μm z-stack (15 × 0.2 μm z steps with 60 ms exposures) was acquired. All images were deconvolved in Nikon Elements. For figure preparation, look up tables were optimized to facilitate visualization.

### *Quantification and statistical analysis*

All images were processed and analyzed using Nikon Elements software or FIJI (https://fiji.sc/).

*Analysis of individual Myo10MD puncta after ATP depletion*—Fiji's TrackMate was used to quantify the sum intensity of individual puncta, run with the following parameters: all frames were included, DoG detector, 0.5 μm diameter with a 0.75 quality threshold, no initial thresholding restrictions, LAP tracker, 1.0 μm max distance frame linking, and allow gap closing with a max distance of 0.5 μm with a max gap frame of 2. Puncta were discounted if present in the initial image prior to ATP depletion, and puncta were only included if they remained in frame for 15 or more frames. An average was calculated from the sum intensity of each punctum over all frames in which it appeared. For background sampling, the same sized region of interest from TrackMate was used to measure 100 points of background intensity from each of the four separate imaging days used for data collection.

*Analysis of the number of motors at the tips of filopodia*—A 2 × 2 μm crop containing a filopodial tip was thresholded using the green, Myo10MD, channel in Nikon Elements and used to generate a background subtracted sum intensity of the entire tip volume. This value was divided by the single molecule calibration intensity (320 12 bit intensity units) to calculate the number of Myo10MD molecules in each tip. Radial plots of the $SunTag_{18x}$-filoForm were generated using OriginPro.

*Measuring the dynamics of induced filopodia*—Filopodial length, elongation velocity, and persistence were analyzed with "Track binaries" in Nikon Elements using Myo10MD tip intensity as the fiducial mark. Maximum lengths were measured using line length (length of a straight line from the track origin to the last point). Velocity of individual filopodia was determined by dividing the maximum line length by the time to reach that length. Persistence was measured as the final line length divided by the total path length.

*Statistical analysis*—We generated SuperPlots (48) with the goal of communicating variability between cells (large data points) and between individual filopodia (small data points). All experiments were completed at least in triplicate, and the number of biological replicates (n) in each case is defined in each figure legend. Statistical significance was tested using the unpaired Student's *t* test for comparisons and the paired Student's *t* test for comparisons of the sum intensities of punctum without and with ATP depletion and for the number of motors at filopodial tips. All statistical analyses were performed using PRISM v.10.0.2 (GraphPad).

## Data availability

Raw data generated during the experiments described in this article are available upon request to the corresponding author, Dr Matthew J. Tyska (matthew.tyska@vanderbilt.edu).

*Supporting information*—This article contains supporting information.

*Acknowledgments*—The authors would like to thank all members of the Tyska laboratory for their feedback and guidance. We also acknowledge the Lacks family and are grateful for the use of HeLa cells, which heavily contributed to the discoveries in this work.

*Author contributions*—G.N.F. and M.J.T. writing–review & editing; G.N.F. and M.J.T. writing–original draft; G.N.F. visualization; G.N.F. validation; G.N.F. and M.J.T. methodology; G.N.F. investigation; G.N.F. and M.J.T. formal analysis; G.N.F. data curation; G.N.F. and M.J.T. conceptualization; M.J.T. supervision; G.N.F. and M.J.T. funding acquisition; G.N.F. resources.

*Funding and additional information*—This work was supported by the National Institutes of Health (NIH) NIDDK National Research Service Award F31-DK130599 (G.N.F.) and NIH grants R01 DK125546, R01 DK095811, and R01 DK111949 (M.J.T.). The content is solely the responsibility of the authors and does not necessarily represent the official views of the National Institutes of Health.

*Conflict of interest*—The authors declare no conflict of interest with the contents of this article.

*Abbreviations*—The abbreviations used are: DMEM, Dulbecco's modified Eagle's medium; FBS, fetal bovine serum; Myo10FL, full-length Myo10; Myo10MD, myosin-10 motor domain; SDCM, spinning disk confocal microscopy.

## References

1. Houdusse, A., and Titus, M. A. (2021) The many roles of myosins in filopodia, microvilli and stereocilia. *Curr. Biol.* **31**, R586–R602
2. Vignjevic, D., Kojima, S., Aratyn, Y., Danciu, O., Svitkina, T., and Borisy, G. G. (2006) Role of fascin in filopodial protrusion. *J. Cell Biol.* **174**, 863–875
3. Wood, W., Jacinto, A., Grose, R., Woolner, S., Gale, J., Wilson, C., *et al.* (2002) Wound healing recapitulates morphogenesis in Drosophila embryos. *Nat. Cell Biol.* **4**, 907–912
4. Fierro-Gonzalez, J. C., White, M. D., Silva, J. C., and Plachta, N. (2013) Cadherin-dependent filopodia control preimplantation embryo compaction. *Nat. Cell Biol.* **15**, 1424–1433
5. Portera-Cailliau, C., Pan, D. T., and Yuste, R. (2003) Activity-regulated dynamic behavior of early dendritic protrusions: evidence for different types of dendritic filopodia. *J. Neurosci.* **23**, 7129–7142
6. Kovar, D. R., and Pollard, T. D. (2004) Insertional assembly of actin filament barbed ends in association with formins produces piconewton forces. *Proc. Natl. Acad. Sci. U. S. A.* **101**, 14725–14730
7. Mogilner, A., and Rubinstein, B. (2005) The physics of filopodial protrusion. *Biophysical J.* **89**, 782–795
8. Theriot, J. A. (2000) The polymerization motor. *Traffic* **1**, 19–28
9. McConnell, R. E., Benesh, A. E., Mao, S., Tabb, D. L., and Tyska, M. J. (2011) Proteomic analysis of the enterocyte brush border. *Am. J. Physiol. - Gastrointest. Liver Physiol.* **300**, 6914–6926
10. Jacquemet, G., Stubb, A., Saup, R., Miihkinen, M., Kremneva, E., Hamidi, H., *et al.* (2019) Filopodome mapping identifies p130Cas as a mechanosensitive regulator of filopodia stability. *Curr. Biol.* **29**, 202–216.e207
11. Krey, J. F., Wilmarth, P. A., David, L. L., and Barr-Gillespie, P. G. (2017) Analysis of the proteome of hair-cell stereocilia by mass spectrometry. *Methods Enzymol.* **585**, 329–354
12. Berg, J. S., and Cheney, R. E. (2002) Myosin-X is an unconventional myosin that undergoes intrafilopodial motility. *Nat. Cell Biol.* **4**, 246–250
13. Chen, Z. Y., Hasson, T., Zhang, D. S., Schwender, B. J., Derfler, B. H., Mooseker, M. S., *et al.* (2001) Myosin-VIIb, a novel unconventional myosin, is a constituent of microvilli in transporting epithelia. *Genomics* **72**, 285–296
14. Belyantseva, I. A., Boger, E. T., and Friedman, T. B. (2003) Myosin XVa localizes to the tips of inner ear sensory cell stereocilia and is essential for staircase formation of the hair bundle. *Proc. Natl. Acad. Sci. U. S. A.* **100**, 13958–13963
15. Hasson, T., Heintzelman, M. B., Santos-Sacchi, J., Corey, D. P., and Mooseker, M. S. (1995) Expression in cochlea and retina of myosin VIIa, the gene product defective in Usher syndrome type 1B. *Proc. Natl. Acad. Sci. U. S. A.* **92**, 9815–9819
16. Petersen, K. J., Goodson, H. V., Arthur, A. L., Luxton, G. W., Houdusse, A., and Titus, M. A. (2016) MyTH4-FERM myosins have an ancient and conserved role in filopod formation. *Proc. Natl. Acad. Sci. U. S. A.* **113**, E8059–E8068
17. Popovic, A., Miihkinen, M., Ghimire, S., Saup, R., Gronloh, M. L. B., Ball, N. J., *et al.* (2023) Myosin-X recruits lamellipodin to filopodia tips. *J. Cell Sci.* **136**, jcs260574
18. Tokuo, H., and Ikebe, M. (2004) Myosin X transports Mena/VASP to the tip of filopodia. *Biochem. Biophys. Res. Commun.* **319**, 214–220
19. Wei, Z., Yan, J., Lu, Q., Pan, L., and Zhang, M. (2011) Cargo recognition mechanism of myosin X revealed by the structure of its tail MyTH4-FERM tandem in complex with the DCC P3 domain. *Proc. Natl. Acad. Sci. U. S. A.* **108**, 3572–3577
20. Zhang, H., Berg, J. S., Li, Z., Wang, Y., Lang, P., Sousa, A. D., *et al.* (2004) Myosin-X provides a motor-based link between integrins and the cytoskeleton. *Nat. Cell Biol.* **6**, 523–531
21. Zhu, X. J., Wang, C. Z., Dai, P. G., Xie, Y., Song, N. N., Liu, Y., *et al.* (2007) Myosin X regulates netrin receptors and functions in axonal path-finding. *Nat. Cell Biol.* **9**, 184–192
22. Sun, Y., Sato, O., Ruhnow, F., Arsenault, M. E., Ikebe, M., and Goldman, Y. E. (2010) Single-molecule stepping and structural dynamics of myosin X. *Nat. Struct. Mol. Biol.* **17**, 485–491
23. Fitz, G. N., Weck, M. L., Bodnya, C., Perkins, O. L., and Tyska, M. J. (2023) Protrusion growth driven by myosin-generated force. *Dev. Cell* **58**, 18–33.e16
24. Eddington, C., Schwartz, J. K., and Titus, M. A. (2024) filovision - using deep learning and tip markers to automate filopodia analysis. *J. Cell Sci.* **137**, jcs261274
25. Urbancic, V., Butler, R., Richier, B., Peter, M., Mason, J., Livesey, F. J., *et al.* (2017) Filopodyan: an open-source pipeline for the analysis of filopodia. *J. Cell Biol.* **216**, 3405–3422
26. Jacquemet, G., Hamidi, H., and Ivaska, J. (2019) Filopodia quantification using FiloQuant. *Methods Mol. Biol.* **2040**, 359–373
27. Tanenbaum, M. E., Gilbert, L. A., Qi, L. S., Weissman, J. S., and Vale, R. D. (2014) A protein-tagging system for signal amplification in gene expression and fluorescence imaging. *Cell* **159**, 635–646
28. Ershov, D., Phan, M. S., Pylvanainen, J. W., Rigaud, S. U., Le Blanc, L., Charles-Orszag, A., *et al.* (2022) TrackMate 7: integrating state-of-the-art segmentation algorithms into tracking pipelines. *Nat. Methods* **19**, 829–832
29. Liu, H., Dong, P., Ioannou, M. S., Li, L., Shea, J., Pasolli, H. A., *et al.* (2018) Visualizing long-term single-molecule dynamics in vivo by stochastic protein labeling. *Proc. Natl. Acad. Sci. U. S. A.* **115**, 343–348
30. Dufourt, J., Bellec, M., Trullo, A., Dejean, M., De Rossi, S., Favard, C., *et al.* (2021) Imaging translation dynamics in live embryos reveals spatial heterogeneities. *Science* **372**, 840–844
31. Tyska, M. J., and Mooseker, M. S. (2002) MYO1A (brush border myosin I) dynamics in the brush border of LLC-PK1-CL4 cells. *Biophys. J.* **82**, 1869–1883
32. Tinevez, J. Y., Perry, N., Schindelin, J., Hoopes, G. M., Reynolds, G. D., Laplantine, E., *et al.* (2017) TrackMate: an open and extensible platform for single-particle tracking. *Methods* **115**, 80–90
33. Shangguan, J., and Rock, R. S. (2023) Pushed to the edge: hundreds of Myosin 10s pack into filopodia and could cause traffic jams on actin. *bioRxiv*
34. VanBuren, P., Work, S. S., and Warshaw, D. M. (1994) Enhanced force generation by smooth muscle myosin in vitro. *Proc. Natl. Acad. Sci. U. S. A.* **91**, 202–205

35. Homma, K., and Ikebe, M. (2005) Myosin X is a high duty ratio motor. *J. Biol. Chem.* **280**, 29381–29391
36. Kovacs, M., Wang, F., and Sellers, J. R. (2005) Mechanism of action of myosin X, a membrane-associated molecular motor. *J. Biol. Chem.* **280**, 15071–15083
37. Inobe, T., and Nukina, N. (2016) Rapamycin-induced oligomer formation system of FRB-FKBP fusion proteins. *J. Biosci. Bioeng.* **122**, 40–46
38. Footer, M. J., Kerssemakers, J. W., Theriot, J. A., and Dogterom, M. (2007) Direct measurement of force generation by actin filament polymerization using an optical trap. *Proc. Natl. Acad. Sci. U. S. A.* **104**, 2181–2186
39. Lewis, A. K., and Bridgman, P. C. (1992) Nerve growth cone lamellipodia contain two populations of actin filaments that differ in organization and polarity. *J. Cell Biol.* **119**, 1219–1243
40. Winkelman, J. D., Bilancia, C. G., Peifer, M., and Kovar, D. R. (2014) Ena/VASP Enabled is a highly processive actin polymerase tailored to self-assemble parallel-bundled F-actin networks with Fascin. *Proc. Natl. Acad. Sci. U. S. A.* **111**, 4121–4126
41. Sheetz, M. P. (2001) Cell control by membrane-cytoskeleton adhesion. *Nat. Rev. Mol. Cell Biol.* **2**, 392–396
42. Sheetz, M. P., Wayne, D. B., and Pearlman, A. L. (1992) Extension of filopodia by motor-dependent actin assembly. *Cell Motil. Cytoskeleton* **22**, 160–169
43. Shi, Z., Graber, Z. T., Baumgart, T., Stone, H. A., and Cohen, A. E. (2018) Cell membranes resist flow. *Cell* **175**, 1769–1779.e1713
44. Dobramysl, U., Jarsch, I. K., Inoue, Y., Shimo, H., Richier, B., Gadsby, J. R., *et al.* (2021) Stochastic combinations of actin regulatory proteins are sufficient to drive filopodia formation. *J. Cell Biol.* **220**, e202003052
45. Ropars, V., Yang, Z., Isabet, T., Blanc, F., Zhou, K., Lin, T., *et al.* (2016) The myosin X motor is optimized for movement on actin bundles. *Nat. Commun.* **7**, 12456
46. Mirdita, M., Schutze, K., Moriwaki, Y., Heo, L., Ovchinnikov, S., and Steinegger, M. (2022) ColabFold: making protein folding accessible to all. *Nat. Methods* **19**, 679–682
47. Medalia, O., Beck, M., Ecke, M., Weber, I., Neujahr, R., Baumeister, W., *et al.* (2007) Organization of actin networks in intact filopodia. *Curr. Biol.* **17**, 79–84
48. Lord, S. J., Velle, K. B., Mullins, R. D., and Fritz-Laylin, L. K. (2020) SuperPlots: communicating reproducibility and variability in cell biology. *J. Cell Biol.* **219**, e202001064